PFC/JA-83-35

Influx and Sources of Medium and High Z Intrinsic Impurities in the Alcator C Tokamak

J. E. Rice, E. S. Marmar, B. Lipschultz, J. L. Terry

Plasma Fusion Center
Massachusetts Institute of Technology
Cambridge, MA 02139

October 1983

This work was supported by the U.S. Department of Energy Contract No. DE-AC02-78ET51013. Reproduction, translation, publication, use and disposal, in whole or in part by or for the United States government is permitted.

INFLUX AND SOURCES OF MEDIUM AND HIGH Z INTRINSIC IMPURITIES IN THE ALCATOR C TOKAMAK

J. E. Rice, E. S. Marmar, B. Lipschultz and J. L. Terry
Plasma Fusion Center
Massachusetts Institute of Technology
Cambridge, MA 02139

Abstract

The influx of heavy impurities in the Alcator C tokamak has been determined as a function of plasma parameters from observations of intrinsic impurities, in conjunction with an empirically derived anomalous impurity diffusion model. The influx of molybdenum as a function of electron density is found to decrease dramatically as the electron density is raised above 1×10^{14} cm^{-3}. Sputtering (by neutrals, ions and impurities) is probably the dominant molybdenum release mechanism in ohmically heated discharges.

1. Introduction

Heavy impuritiy densities must be minimized in fusion reactors due to the radiation cooling they would cause. While the very long impurity confinement time predicted by neoclassical theory is generally not observed in reasonably clean, ohmically heated tokamak discharges, it would be desirable not to have impurities in the first place. This requires an ability to control the impurities at their source. In order to limit the source, the physical origins at the plasma edge must first be located, and attempts made to understand the mechanisms responsible for impurity generation there. In plasmas with strong auxilliary heating, long impurity

confinement times are sometimes observed [1]. If these cases are unavoidable, it becomes extremely important to reduce the impurity influx. It is the purpose of this study to utilize observations of instrinsic impurities in the Alcator C tokamak to obtain a better understanding of the plasma-wall interactions and the resultant impurity generation and influx into the hot core of tokamak plasmas.

If the transport which takes impurities from the edge to the interior plasma is understood, then their source can be characterized from observations of these impurities in the plasma. An empirical impurity transport coefficient, determined from a series of trace impurity injection experiments, and a computer code used to model these results, are reviewed in section 2. Observations of intrinsic molybdenum, chlorine and sulphur, as well as predictions from the transport model are presented in section 3. The deduced scalings of the influx of these impurities are presented in section 4, comments about the effects of changes in edge plasma parameters are given in section 5 and some speculations about the mechanisms which remove the impurities from the walls and limiters are offered in section 6.

2. Review of impurity injection experiments on Alcator C

A series of impurity injection experiments has been performed on the Alcator C tokamak [2] in order to determine the nature of impurity transport. The results of these injections were found to be inconsistent with the predictions of pure neo-classical impurity transport [3]. The observations were, however, well described by a model which includes only the effects of self-diffusion. The density of a particular ionization state

can be found from

$$\frac{\partial n_j}{\partial t} = -\frac{1}{r}\frac{\partial}{\partial r}(r\Gamma_j) + n_e[s_{j-1}n_{j-1} - s_j n_j + \alpha_j n_{j+1} - \alpha_{j-1}n_j] + \text{source} \quad (1)$$

with the flux given by

$$\Gamma_j = -d\frac{\partial n_j}{\partial r}. \quad (2)$$

S_j is the ionization rate from, and α_j is the recombination (radiative and dielectronic) rate to the j^{th} state. Code predictions (Eqs. 1 and 2) use a delta function source to model the injection process. The observed time histories of particular charge states yield the anomalous impurity diffusion coefficient, d, whose scalings with plasma parameters were found to be

$$d(cm^2/sec) = \frac{2300\ a_L\ q_L}{R^{\cdot 75}\ m_{bg}}\ (Z_{bg}/Z_{eff}) \quad (3)$$

a_L and R are the minor and major radii (in cm), q_L is the limiter safety factor, M_{bg} is the background ion mass (in amu), Z_{bg} is the background ion charge and Z_{eff} is the effective charge of the plasma due to intrinsic impurities. This diffusion coefficient is independent of electron density, provided there are only low levels of MHD activity. In addition, the coefficient does not depend on the charge and mass of the impurity, provided the impurity's presence does not disturb the macroscopic plasma parameters. While the dependences on major radius and Z_{eff} should not be taken as strict scaling laws, the other variations are quite well established empirically.

From a known source and measured impurity emission, the impurity transport thus has been determined. Alternatively, given the impurity transport and measured impurity emission, the source of intrinsic impurities can be characterized.

3. Observed scalings of molybdenum, chlorine and sulphur

Intrinsic impurity emission from Alcator C is routinely monitored with a flat crystal x-ray spectrometer employing a PET crystal (1 Å < λ < 8 Å) and with a 1 m. grazing incidence monochromator (40 Å < λ < 550 Å). The dominant medium and high Z impurities are molybdenum, chlorine, sulphur, chromium and iron [4,5,6]. Data have been collected under a wide range of operating conditions: 10^{13} cm^{-3} < $\bar{n}_e$ < 10^{15} cm^{-3}; 200 kA < I < 700 kA; 60 kG < B_t < 120 kG; in hydrogen, deuterium and helium working gases; and with three limiter configurations (10 cm molybdenum, 16.5 cm molybdenum and 16.5 cm graphite).

A typical scaling of molybdenum emission as a function of electron density is shown in fig. 1. The steady state brightness at 77 Å, in the middle of a quasi-continuum of lines due to charge states near Mo^{25+} [7,8] is plotted for a sequence of 200 kA, 120 kG deuterium discharges. In this case, the minor radius was 10 cm, defined by a molybdenum limiter, and the wall-to-limiter distance was 9 cm. The molybdenum brightness rapidly increases with decreasing electron density below about 2×10^{14} cm^{-3}. A similar situation is inferred from the x-ray observations, as depicted in fig. 2. The brightness, with the background subtracted, at 5.2 Å (2p-3s transition [6,9,10] in Mo^{32+}) is shown as a function of electron density for a series of discharges at 415 kA and 80 kG in deuter-

ium. In this example, the minor radius was 16.5 cm and the limiter material was graphite, indicating that the source of molybdenum was either the walls (r = 19 cm) or the virtual limiters (r = 17.5 cm). The graphite limiters were installed after about 3 years of operation with molybdenum limiters. Again, there is a marked increase in molybdenum brightness below electron densities of 2×10^{14} cm^{-3}. This increase is accompanied by rapid increases in total radiated power [11], Z_{eff} and electron temperature as shown in fig. 3. The electron temperature was measured with a Si(Li) detector and pulse height analysis system.

The behavior of chlorine is somewhat different. Shown in fig. 4(a) are the time histories of He-like chlorine (4.44 Å), the central chord line-averaged electron density ($.58 \times 10^{14}$ cm^{-3}/fringe) and the central chord soft x-ray brightness ($h\nu \gtrsim 1$ keV). The chlorine brightness seems to follow the electron density, and is nearly constant between 150 and 375 ms. Contrast the case of He-like sulphur (5.039 Å) shown in fig. 4(b) for a similar (the next) discharge. Here the emission seems to track the soft x-ray signal (also the molybdenum signal), increasing monotonically until 350 ms. The atomic processes of these two adjacent ions are similar, and the transport has been shown to be independent of impurity species. The physical source of these impurities may be the same, since the signal levels of both sulphur and chlorine dropped a factor of 8 or so when the limiter was changed from molybdenum to graphite. The difference in the time histories of their He-like emissions must be due to differences in the mechanisms responsible for their removal from the same surfaces. The scaling of the He-like chlorine signal with electron density is shown in fig. 5 for deuterium discharges with a 10 cm molybdenum limiter. Toroidal magnetic field and plasma current have been

kept constant over this density scan. In contrast to the molybdenum scaling, the chlorine brightness increases nearly linearly with electron density for $\bar{n}_e > 2 \times 10^{14}$ cm^{-3}. It is difficult to measure emission from He-like chlorine below this density since there are molybdenum lines at the same wavelength which dominate. In contrast, there are no molybdenum scaling data above 2.5×10^{14} cm^{-3}, since molybdenum radiation is undetectable above the x-ray continuum.

The variation of the x-ray molybdenum brightness at 5.2 Å as a function of plasma current is shown in fig. 6 for a series of 100 kG, deuterium discharges at an electron density of 1.4×10^{14} cm^{-3}. There is a strong increase in the molybdenum brightness as the current is raised from 250 to 600 kA. It should be noted that as the current is increased, the central electron temperature, the electron temperature profile width and the impurity confinement time all increase. As before, the limiters were 16.5 cm graphite.

4. Determination of the molybdenum and chlorine influxes

Since impurity transport is independent of electron density, the brightness of chlorine might be expected to increase linearly with $\bar{n}_e$, provided the chlorine source is also independent of electron density. This is just what is predicted by the transport code described above, assuming a steady state impurity source independent of $\bar{n}_e$. The predicted brightness is shown in fig. 5 by the solid line. In this case, the diffusion coefficient, d, from eq.(3), was 1100 cm^2/sec. The chlorine influx was taken to be independent of electron density and the measured changes in the electron temperature were included.

Contrast the case of molybdenum shown in fig. 6. Since the anomalous diffusion coefficient in eq. (3) is proportional to the limiter safety factor, the impurity confinement time increases with plasma current. It might be expected that the molybdenum brightness should correspondingly increase with plasma current. Although this notion is qualitatively similar to the observations of fig. 6, a slight variation of the molybdenum influx with plasma current is required to achieve quantitative agreement. By scaling the diffusion coefficient with current in accordance with eq. (3), and incorporating the appropriate changes in the electron temperature and profile in eq. (1), the molybdenum source has been adjusted to comply with the data of fig. 6. The result for the variaton of the influx as a function of plasma current is shown in fig. 7. There is a slight decrease in the influx with increasing current but, as will be shown later, changes of this magnitude are not considered significant within this model. The conclusion here is that the increase of molybdenum brightness with increasing plasma current can be mostly accounted for by the increase in impurity confinement with plasma current in accordance with eq.(3).

The dependence of molybdenum influx on electron density can be obtained from the data of fig. 1 or fig. 2 by following a similar procedure to that described above. The molybdenum influx shown as a function of electron density in fig. 8, is obtained from the data of fig. 2. There is a strong decrease in the molybdenum influx as electron density increases from 1×10^{14} cm^{-3} to 2×10^{14} cm^{-3}. Above this density, the magnitude of molybdenum radiation is less than the background. The apparent turnover of the molybdenum influx below $\bar{n}_e = 1 \times 10^{14}$ cm^{-3} should not be taken too seriously, as effects of this magnitude may be due to changes

in edge conditions and uncertainties in the temperature profile. A similar situation is obtained from the 10 cm molybdenum limiter data of fig. 1. It is shown in fig. 9 along with some additional 16.5 cm molybdenum limiter results from x-ray observations. The qualitative trends in figs. 8 and 9 are the same, although the location of the source for fig. 8 was the vacuum chamber walls and/or virtual limiters, while in fig. 9, the source was mainly the limiter. The overall level of molybdenum emission, in otherwise similar discharges, is a factor of ~ 20 greater with molybdenum limiters than with graphite limiters.

When the background gas was changed from deuterium to helium (with $\bar{n}_e = 2.4 \times 10^{14}$ cm^{-3}, $I_p = 300$ kA and $B_t = 80$ kG), the molybdenum brightness at 5.2 Å increased by a factor of 4. Accounting for the enhancement of impurity confinement as the background ion mass is increased (Eq.3), (as well as the slight increase in electron temperature) the predicted increase in signal is about a factor of 6, in rough agreement with what is observed. This indicates that the molybdenum influx is not strongly dependent on the background ion, in changing from deuterium to helium.

5. Effects of edge assumptions

The above conclusions concerning the impurity influx are uncertain by about a factor of 2 because of uncertainties in the edge plasma conditions. Changes in the edge electron density and temperature profiles affect the shape of the deposition profile of the incoming neutral impurities. A typical case for molybdenum is shown in fig. 10, where the ionization rates for MoI from ref. 12 have been used in conjunction with probe measurements of the edge electron density and temperature profiles

[13]. This spatial distribution of the singly ionized impurity (which is also a function of the energy distribution of the incoming MoI) is an initial condition for the transport code (eq.(1)). Variations of this initial profile subsequent to reasonable changes in edge conditions can lead to deviations in the central impurity densities of up to a factor of 2. While this could account for the scalings with plasma current deduced in fig.(7), the conclusions regarding the dependence of the molybdenum influx on electron density remain qualitatively unchanged (except for the apparent turnover below $\bar{n}_e = 1 \times 10^{14}$ cm^{-3} in fig. 8).

6. Interpretations of the instrinsic impurity sources

There are several mechanisms (14) which could remove molybdenum from the walls, limiter and virtual limiters. These include evaporation, physical and chemical sputtering by plasma and impurity ions and neutrals, arcing, blistering and electron desorption. Evaporation of the limiter can occur because a substantial portion of the ohmic heating input is deposited there during each shot. The power density at the limiter during a shot increases nearly linearly with the electron density of the discharge, going from about 250 W/cm^2 at a density of 1×10^{14} cm^{-3} to 900 W/cm^2 at 2×10^{14} cm^{-3} [11]. More evaporation, and hence more molybdenum influx, would be expected as the density is raised, in constrast to what is observed in fig.(8), indicating that evaporation due to thermal edge plasma is not the primary molybdenum introduction process, at least in non-disruptive discharges. Runaway electron induced evaporation is a candidate process since there is sometimes a correlation between molybdenum influx and hard x-ray production for low electron density plasmas. There is not, however, always a good correlation between hard x-ray

production and Mo flux. Non-thermal electrons, generated by RF waves, may be instrumental in introducing impurities during RF heating and current drive experiments [15,16]. Processes such as arcing and blistering presumably introduce molybdenum in discrete bursts in time, a situation similar to the impurity injection experiment. In fact such "natural injections" are seen to occur, as shown in fig. 11. While these events are occasionally observed, they do not result in a steady level of molybdenum emission, which is the routine state of affairs. Sputtering by neutrals is a possible molybdenum release mechanism, since the observed neutral flux, at energies > 1 keV, increases dramatically [17] as the electron density is reduced below 2×10^{14} cm^{-3}. This increase in the neutral flux will give rise to more sputtering and an increase in the molybdenum influx, in qualitative agreement with fig. 8. However, since the molybdenum influx did not change dramatically when the background ion was changed from deuterium to helium, it can be concluded that sputtering by neutrals is not the dominant mechanism in this case. The outflux of energetic neutral helium is much less than the neutral deuterium outflux [17]. This would indicate that sputtering by ions and impurities could be the dominant mechanism. Molybdenum sputtering coefficients are rapidly increasing functions of ion temperature. The edge electron temperature, and presumably the edge ion temperature, increase as the electron density is lowered.

A 1-D edge model [18] has been contructed to explore this hypothesis. The molybdenum sputtering rate due to the flux of background ions to the limiter can be calculated given the edge plasma measurements of electron density and temperature, as well as power to the limiter. Ion and electron temperatures are assumed to be equal. The determination of the sheath

potential follows ref. 19 and sputtering coefficients are evaluated for a given ion energy, mass and charge using DSPUT [20].

The calculated molybdenum influx as a function electron density is shown in fig. 12 for a deuterium plasma with a 16.5 cm limiter. The molybdenum influx, deduced from emission at 5.2 Å in conjunction with the impurity transport model (fig.9), is shown by line A. Line B is the calculated curve for deuterium ions incident on a molybdenum limiter. Although the density dependence is similar for these two source predictions, the discrepency in magnitude cannot be accounted for by the uncertainties in the models. Line C shows the effect of including self sputtering by molybdenum ions. In this case the agreement is reasonable. The increase of the molybdenum influx as the working gas is changed from hydrogen to deuterium to helium may be accounted for by the increase of the sputtering coefficient as the ion mass is increased. The two major uncertainties in this edge model are due to the strong dependence of the sheath potential on the plasma species at the sheath and the assumption of equal ion and electron temperatures at the edge.

The location of the source of molybdenum when operating with a graphite limiter must be the virtual limiters and/or the walls. The electron temperature near these surfaces is low ($\sim$ 5 eV) so sputtering by background ions is unlikely. Sputtering by neutrals and subsequent self sputtering by molybdenum is probably the dominant process under these circumstances. The calculated molybdenum influx due solely to neutral sputtering is shown by line D in fig. 12. The charge-exchange flux to the walls has been computed using the FRANTIC [21] code, and molybdenum was assumed to cover 10% of the walls.

The apparent independence of the chlorine influx on electron density could be due to a combination of competing processes. In particular, the chlorine source could be due mainly to two processes: thermal desorption, which would increase with increasing electron density, since the heat load to the limiter increases; and sputtering, which would decrease with increasing density.

7. Conclusions

Observed intrinsic impurity emission has been combined with an empirically determined transport model in order to characterize the source of impurities in ohmically heated discharges. The influx of molybdenum is found to increase dramatically as the electron density is lowered below 2×10^{14} cm^{-3}. The primary location of the origin of molybdenum, sulphur and chlorine is the molybdenum limiters. The dominant mechanism which removes molybdenum from the limiters is believed to be physical sputtering by plasma ions and self sputtering by molybdenum.

8. Acknowledgements

The authors would like to thank the entire Alcator C group for support and cooperation during these experiments, in particular D. Gwinn and R. Parker for operating the machine, S. Wolfe and R. Gandy for electron density and temperature measurements, B. LaBombard for edge probe measurements, C.Fiore for neutral flux information and K.Chamberlain for assistance in the data reduction.

Figure captions

Fig. 1. Brightness at 77 Å ($\sim Mo^{25+}$) as a function of average electron density, at constant current, with a 10cm molybdenum limiter.

Fig. 2. Brightness at 5.2 Å ($\sim Mo^{32+}$) as a function of electron density, at constant current, with 16.5cm graphite limiters.

Fig. 3. The central electron temperature as a function of average electron density. The curve is parameterized by $T_e = (\bar{n}_e)^{-0.26}$.

Fig. 4. The time histories of helium-like chlorine and sulphur for two sucessive discharges, as well as the electron density and central soft x-ray emission.

Fig. 5. Brightness of helium-like chlorine as a function of electron density. The predicted brightness, assuming a chlorine influx which is independent of electron density, is also shown by the solid line.

Fig. 6. Brightness of neon-like molybdenum as a function of plasma current, at constant electron density, with 16.5cm graphite limiters.

Fig. 7. Molybdenum influx as a function of plasma current inferred from the data of fig. 6. This trend could be due only to changes in edge conditions.

Fig. 8. Molybdenum influx as a function of electron density, with graphite limiters, inferred from the data of fig. 2.

Fig. 9. Molybdenum influx as a function of electron density, with molybdenum limiters, from the data shown in fig. 1 as well as from the

16.5 cm molybdenum limiter case.

Fig. 10. The calculated density profile of Mo^{1+} for typical edge conditions.

Fig. 11. A benign "natural" molybdenum injection.

Fig. 12. Calculated molybdenum influx as a function of electron density. Line A is from fig. 9. Line B is the prediction assuming molybdenum is sputtered by plasma ions only. Line C shows the prediction when molybdenum self sputtering is included. Line D is the source from neutral sputtering only.

References

1. Isler, R. C., L. E. Murray, S. Kasai, D. E. Arnurius, S. C. Bates, et al., Phys. Rev. Lett. 47, (1981) 649.
2. Marmar, E. S., J. E. Rice, J. L. Terry and F. H. Seguin, Nucl. Fusion 22, (1982) 1567.
3. Hawryluk, R. J., Suckewer, S. Hirshman, S. P., Nucl. Fusion 19 (1979) 607.
4. Castracane, J., W. L. Hodge and H. W. Moos, J. Quant. Spect. Rad. Trans. 29, (1983) 157.
5. Kallne, E., J. Kallne and J. E. Rice, Phys. Rev. Lett. 49, (1982) 330.
6. Kallne, E., J. Kallne and R. D. Cowan, Phys. Rev. A. 27 (1983) 2682.
7. Hodge, W. L., J. Castracane, H. W. Moos and E. S. Marmar, J. Quant. Spect. Rad. Trans. 27, (1982) 493.
8. Cowan, R. D., Report LA-6679-MS, LASL, (1976).
9. Burkhalter, P., R. Schneider, C. M. Dozier and R. D. Cowan, Phys. Rev. A 18, (1978) 718.
10. Rice, J. E., E. S. Marmar, T. Coan, S. L. Allen and R. D. Cowan, Phys. Rev. A 22, (1980) 310.
11. Lipschultz, B., A. J. Hayzen, J. Moreno, D. O. Overskei, M. M. Pickrell, et al., Bull. Am. Phys. Soc. 26, (1981) 975.
12. TFR Group, Plasma Physics 19 (1977) 587.
13. LaBombard, B., B. Lipschultz, M. M. Pickrell and Y. Takase, Bull. Am. Phys. Soc. 27, (1982) 1037.
14. McCracken, G. M. and P. E. Stott, Nucl.Fusion 19, (1979) 889.
15. Marmar, E. S., M. Foord, B. LaBombard, B. Lipschultz, J. Moreno, et al., "Impurity Generation during Intense Lower Hybrid Heating Experiments on the Alcator C Tokamak", Jour. of Nucl. Materials to be published, MIT

Plasma Fusion Center Report PFC/JA-83-37, September, 1983.

16. Porkolab, M., et al., 9th Int. Conf. Plas. Res. and Contr. Nucl. Fus. Res., Baltimore, USA, 1982, IAEA-CN-41/C-4.

17. Fiore, C. L. private communicaton (1983).

18. Lipschultz, B., MIT PFC Report PFC/RR-83-24 (1983).

19. Emmert, G. A. et al., Phys. Fluids 23 (1980) 803.

20. Smith, D. L., J. N. Brooks, D. E. Post, D. B. Heifetz, Proceedings of the 9th Symp. on Eng. Probl. of Fus. Res., October, 1981, Chicago, USA

21. Towner, H. H., R. J. Goldston, D. C. McCune, S. Tamor, Bull. Am. Phys. Soc. 26 (1981) 857.

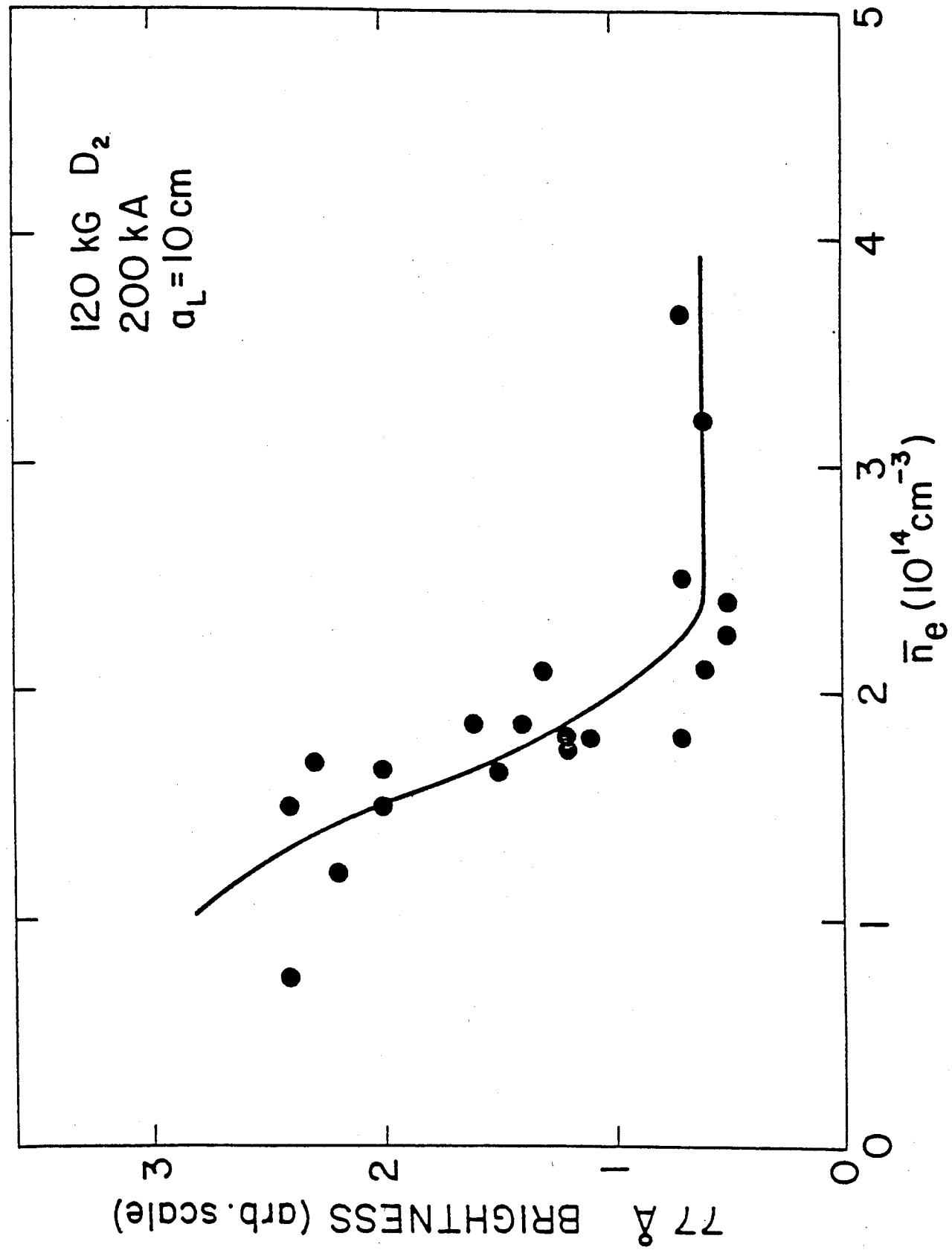
120 kG D_2
200 kA
a_L=10 cm
77 Å BRIGHTNESS (arb. scale)
$\bar{n}_e$ (10^{14} cm^{-3})
0
1
2
3
4
5

FIGURE 1

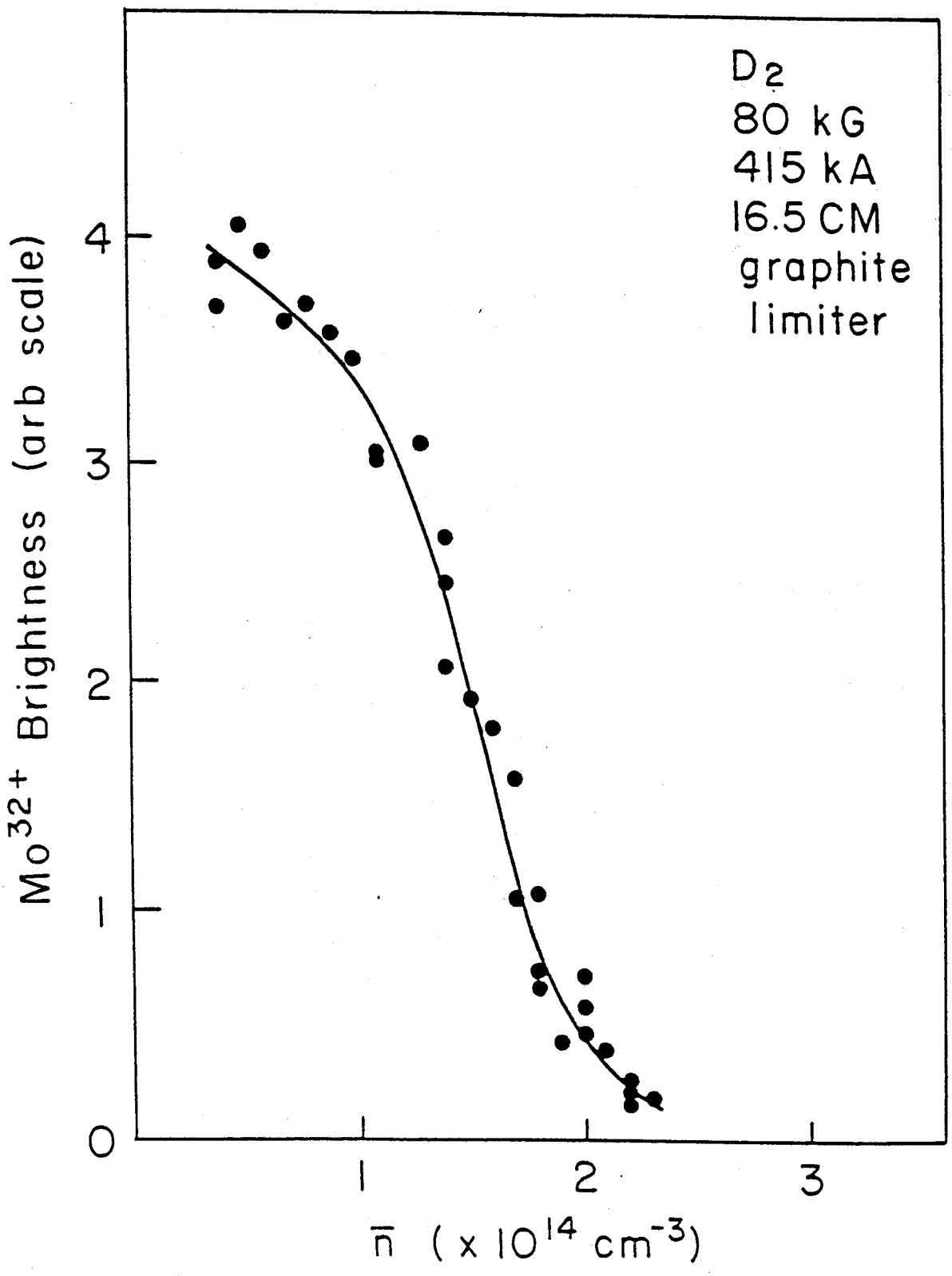
D2
80 kG
415 kA
16.5 CM
graphite
limiter
Mo32+ Brightness (arb scale)
0
1
2
3
4
1
2
3
n̄ (x 10^14 cm^-3)

FIGURE 2

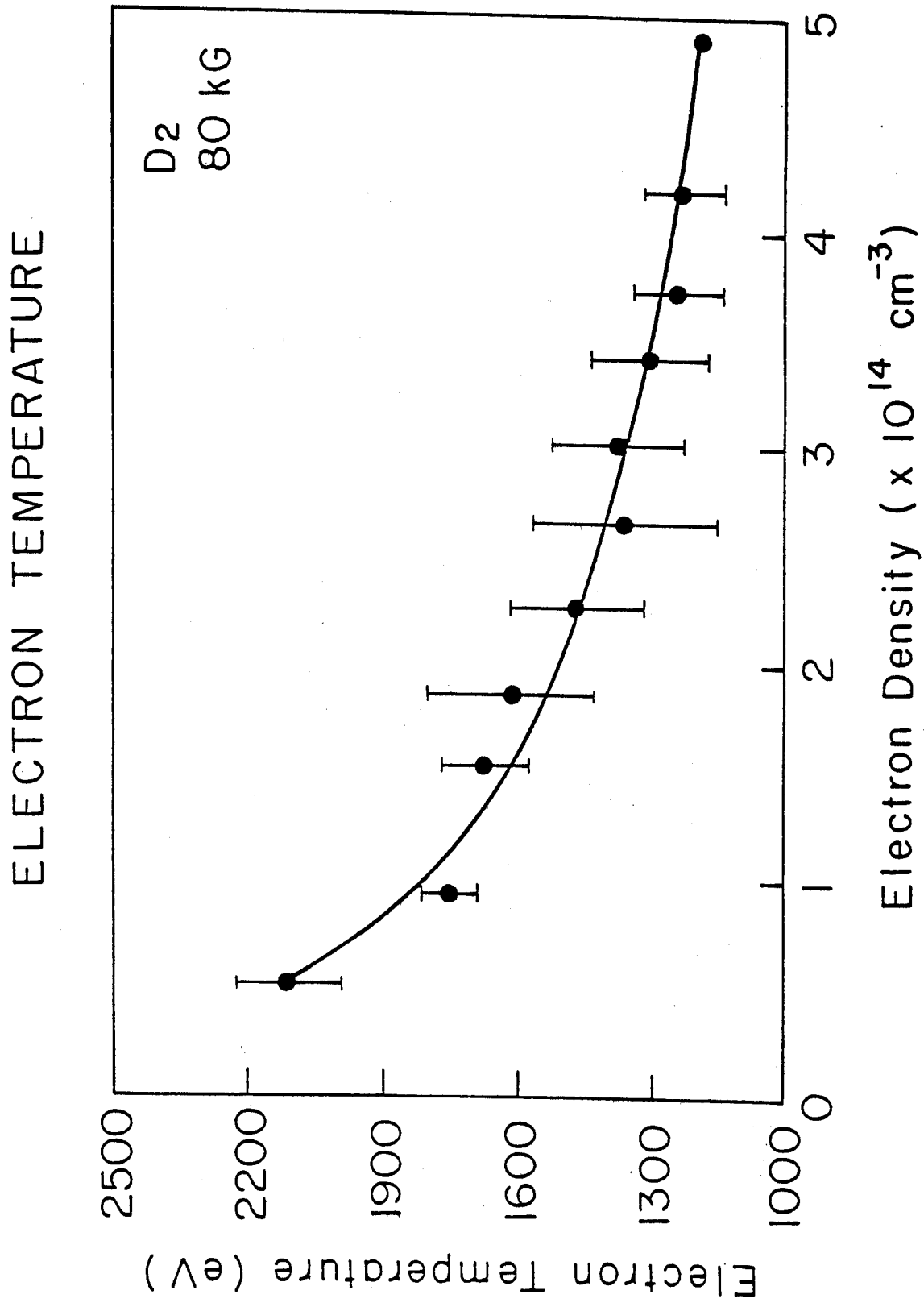
ELECTRON TEMPERATURE
D2
80 kG
Electron Temperature (eV)
2500
2200
1900
1600
1300
1000
0
1
2
3
4
5
Electron Density (x 10^14 cm^-3)

FIGURE 3

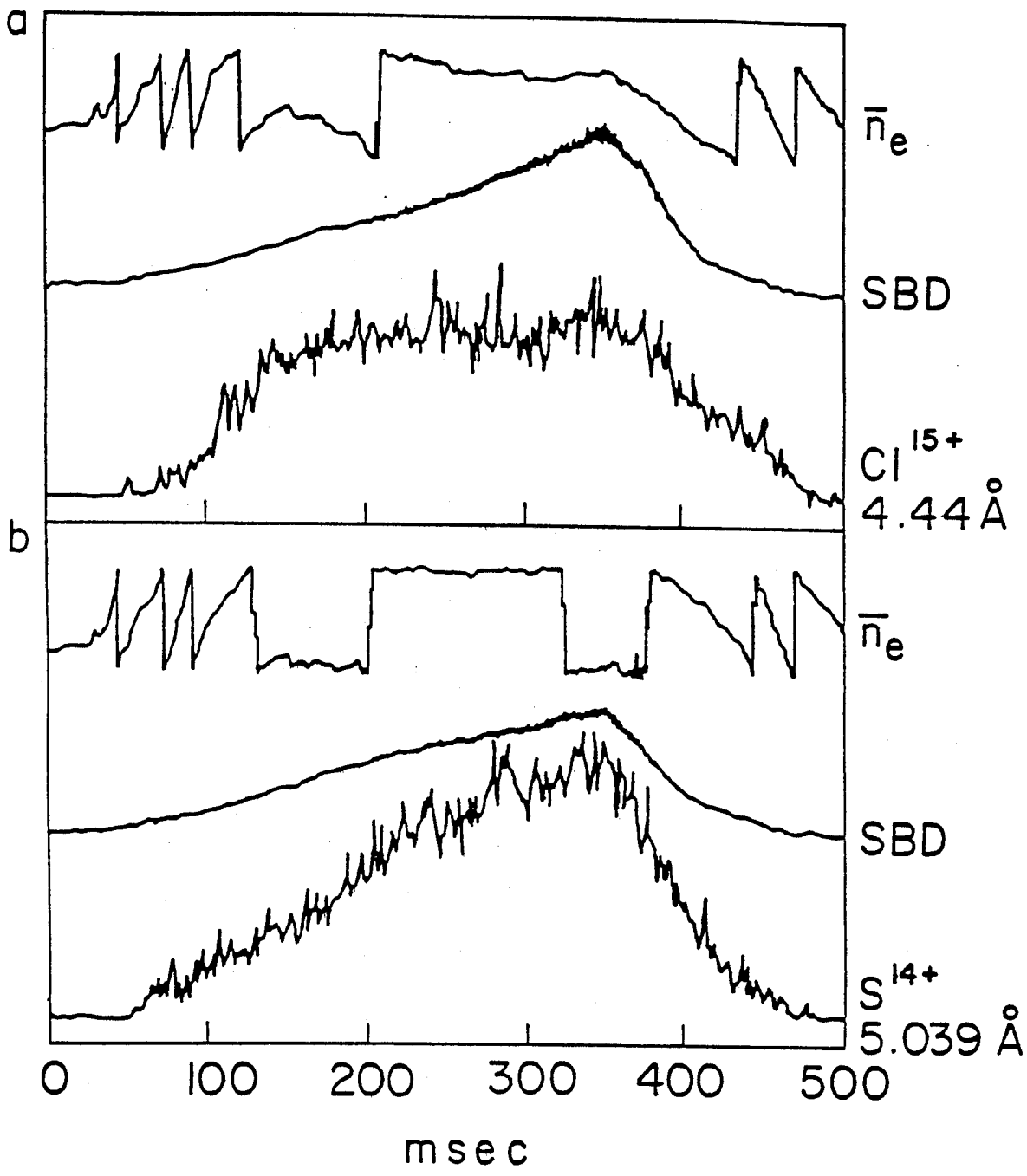
a
$\bar{n}_e$
SBD
Cl^{15+}
4.44 Å
b
$\bar{n}_e$
SBD
S^{14+}
5.039 Å
0
100
200
300
400
500
msec

FIGURE 4

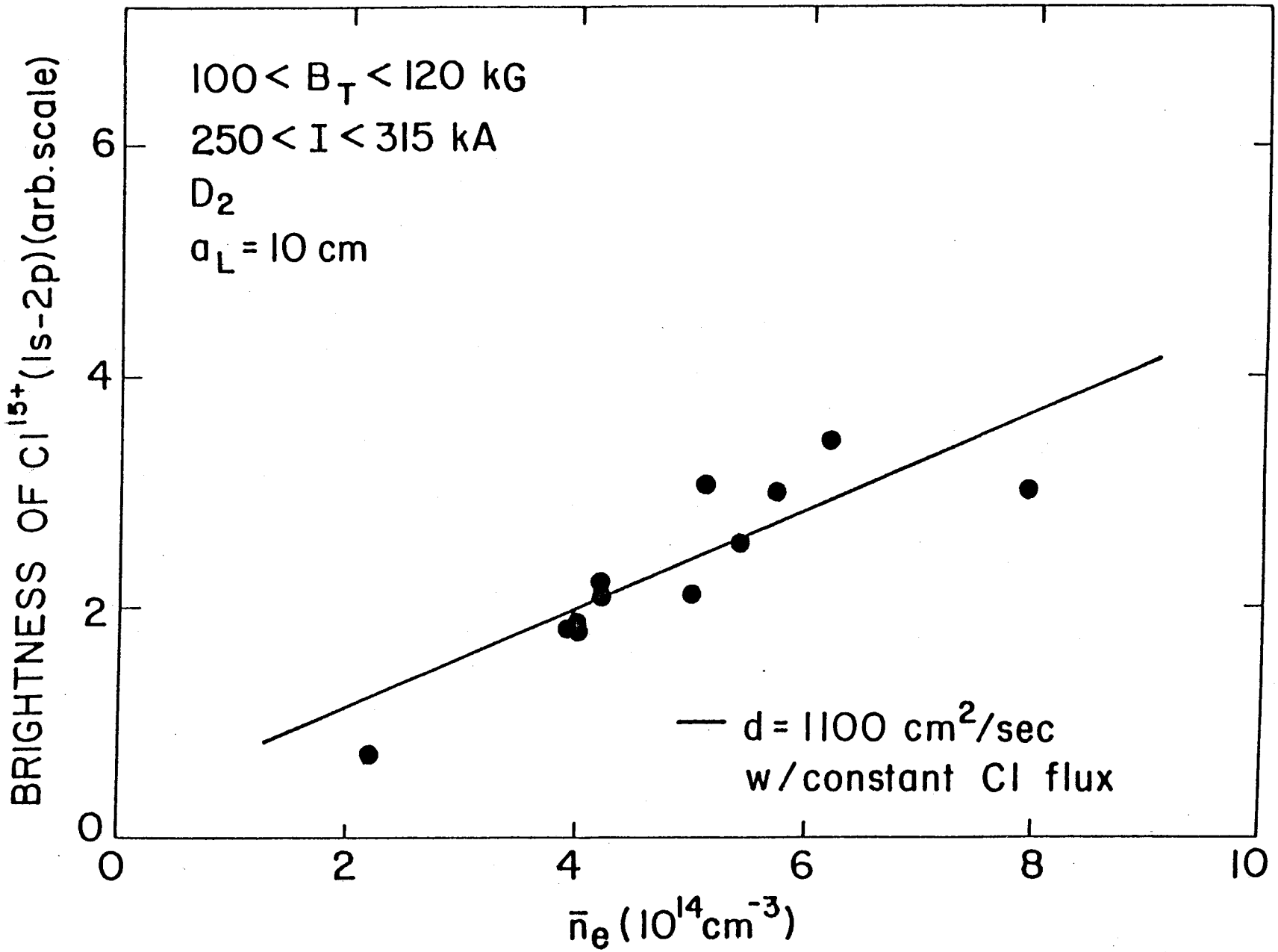
100 < B_T < 120 kG
250 < I < 315 kA
D2
a_L = 10 cm
d = 1100 cm²/sec
w/constant CI flux
BRIGHTNESS OF Cl¹⁵⁺(1s-2p)(arb.scale)
n̄e (10¹⁴cm⁻³)
0
2
4
6
8
10

FIGURE 5

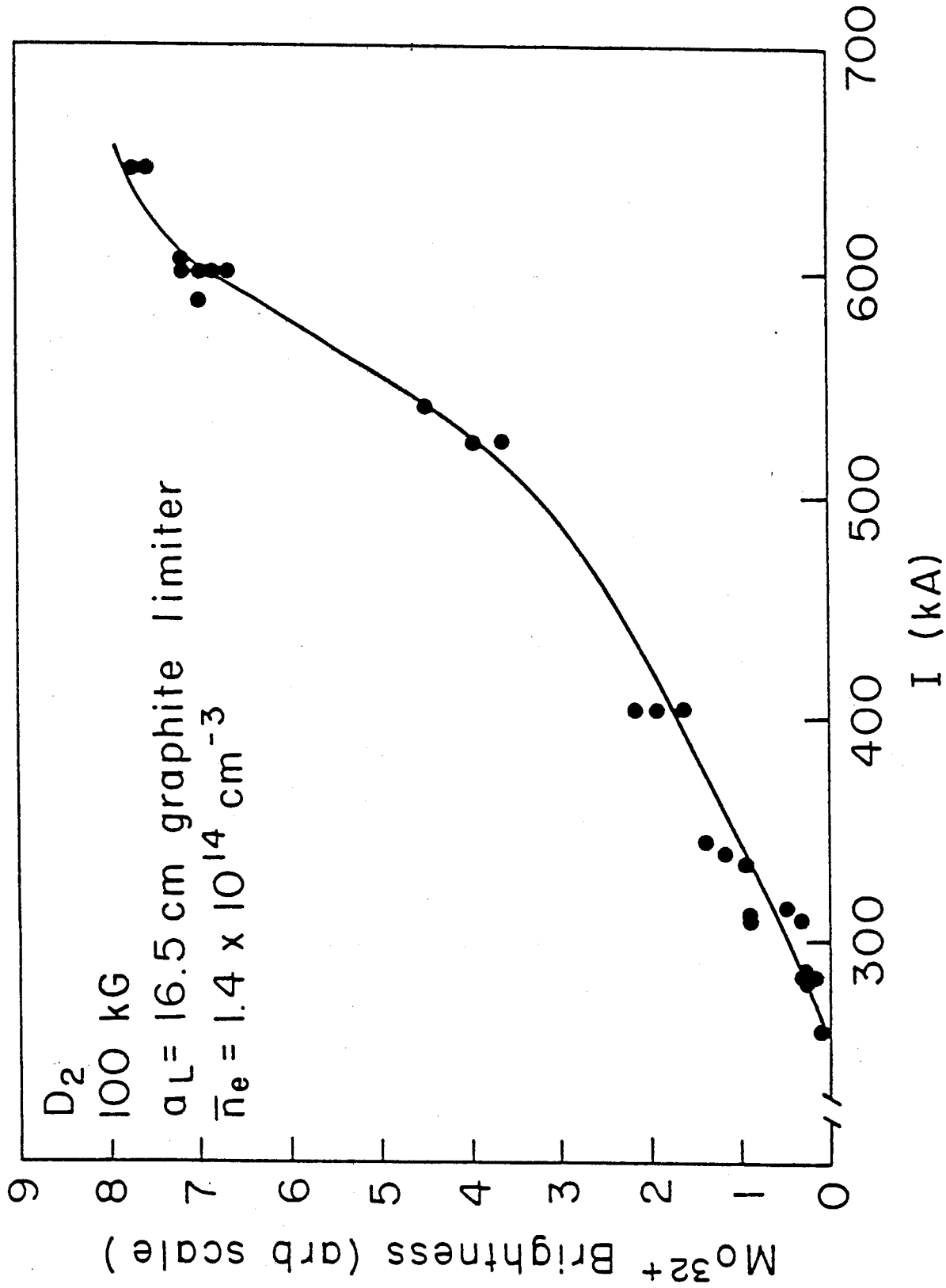
Mo^{32+} Brightness (arb scale)
I (kA)
D_2
100 kG
a_L = 16.5 cm graphite limiter
$\bar{n}_e = 1.4 \times 10^{14}$ cm^{-3}
0
1
2
3
4
5
6
7
8
9
300
400
500
600
700

FIGURE 6

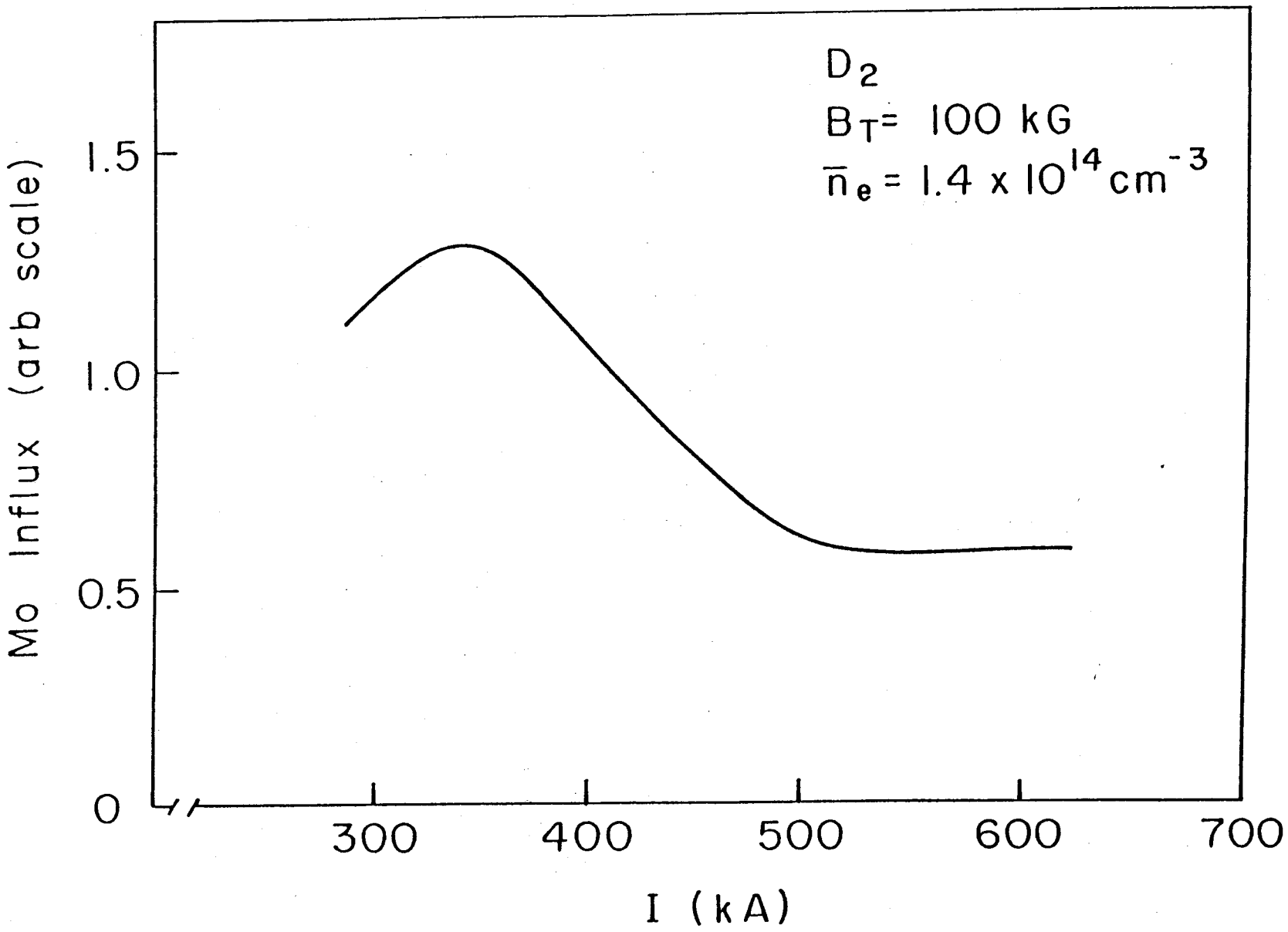
D_2
B_T= 100 kG
$\bar{n}_e = 1.4 \times 10^{14} cm^{-3}$
Mo Influx (arb scale)
1.5
1.0
0.5
0
300
400
500
600
700
I (kA)

FIGURE 7

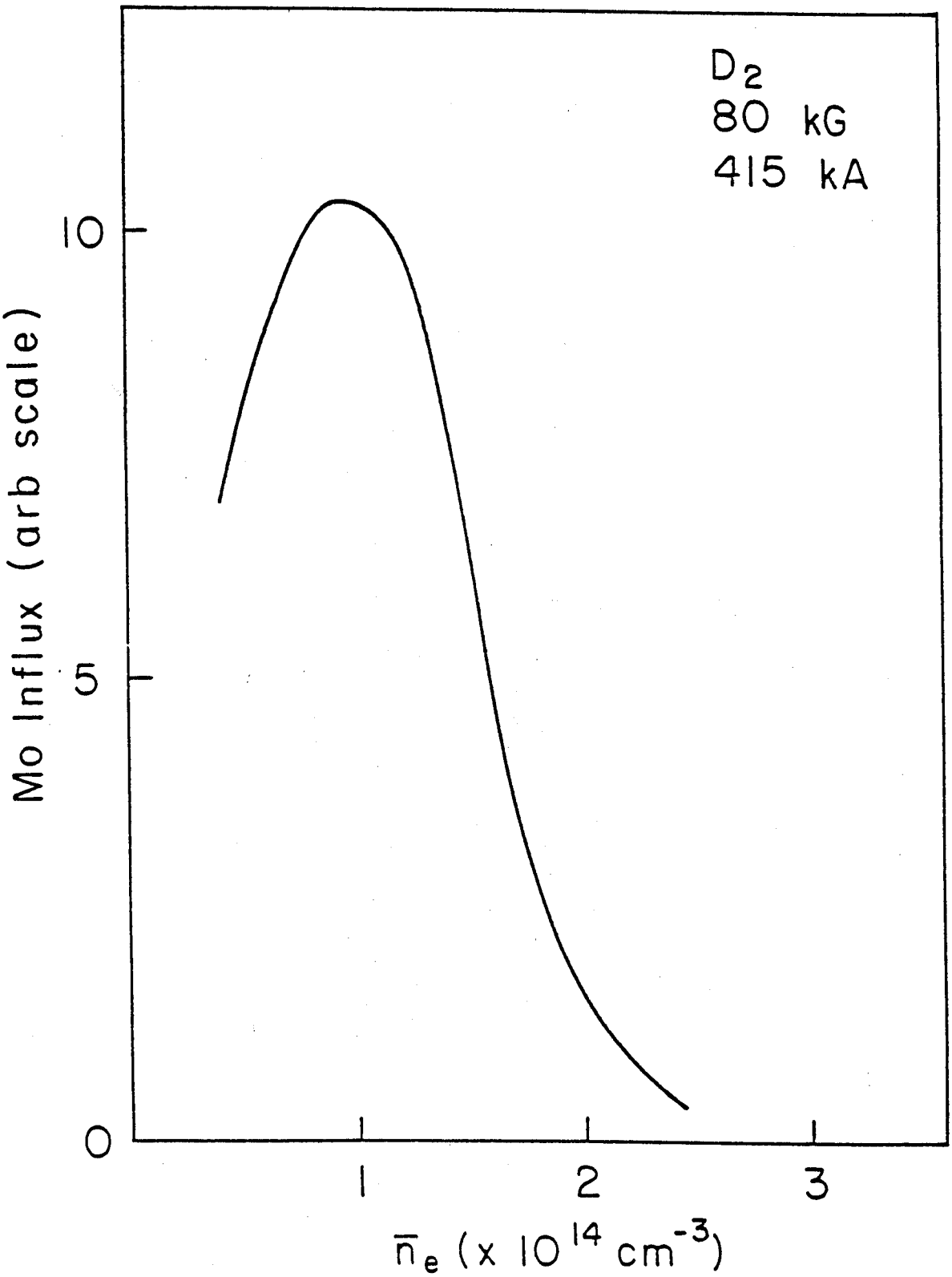

FIGURE 8

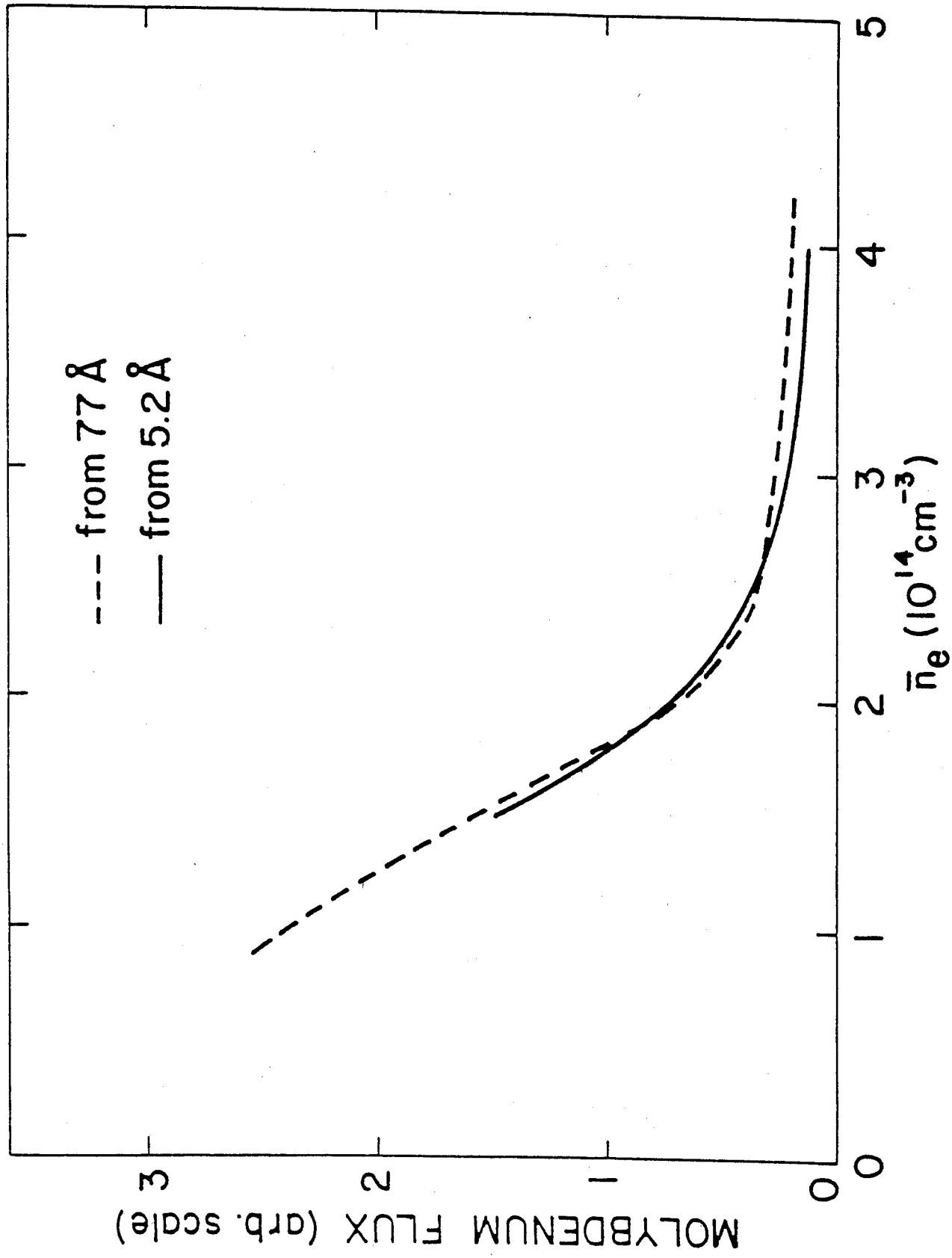
--- from 77 Å
— from 5.2 Å
MOLYBDENUM FLUX (arb. scale)
0
1
2
3
$\bar{n}_e$ (10^{14} cm^{-3})
0
1
2
3
4
5

FIGURE 9

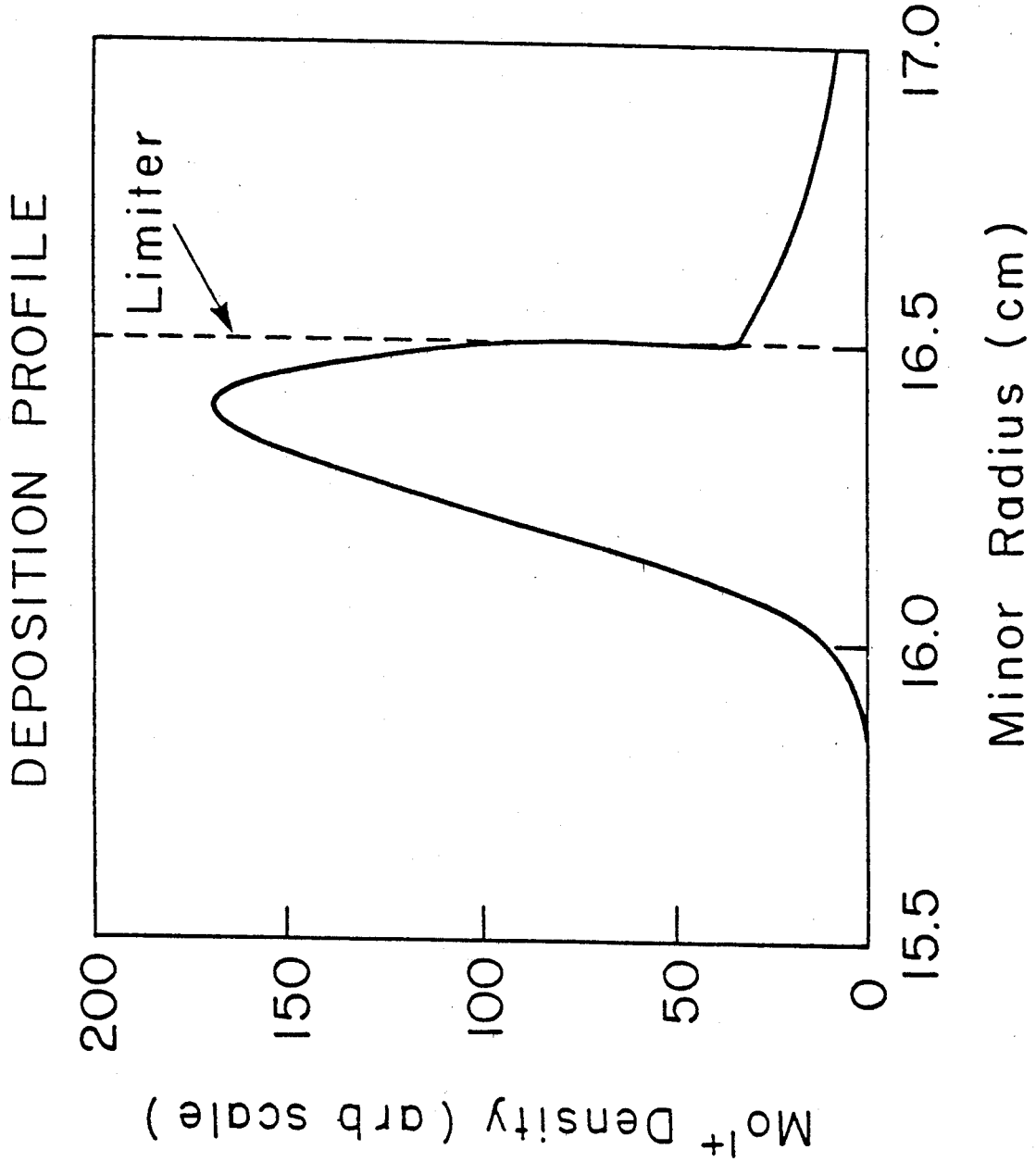
DEPOSITION PROFILE
Limiter
200
150
100
50
0
Mo^{1+} Density (arb scale)
15.5
16.0
16.5
17.0
Minor Radius (cm)

FIGURE 10

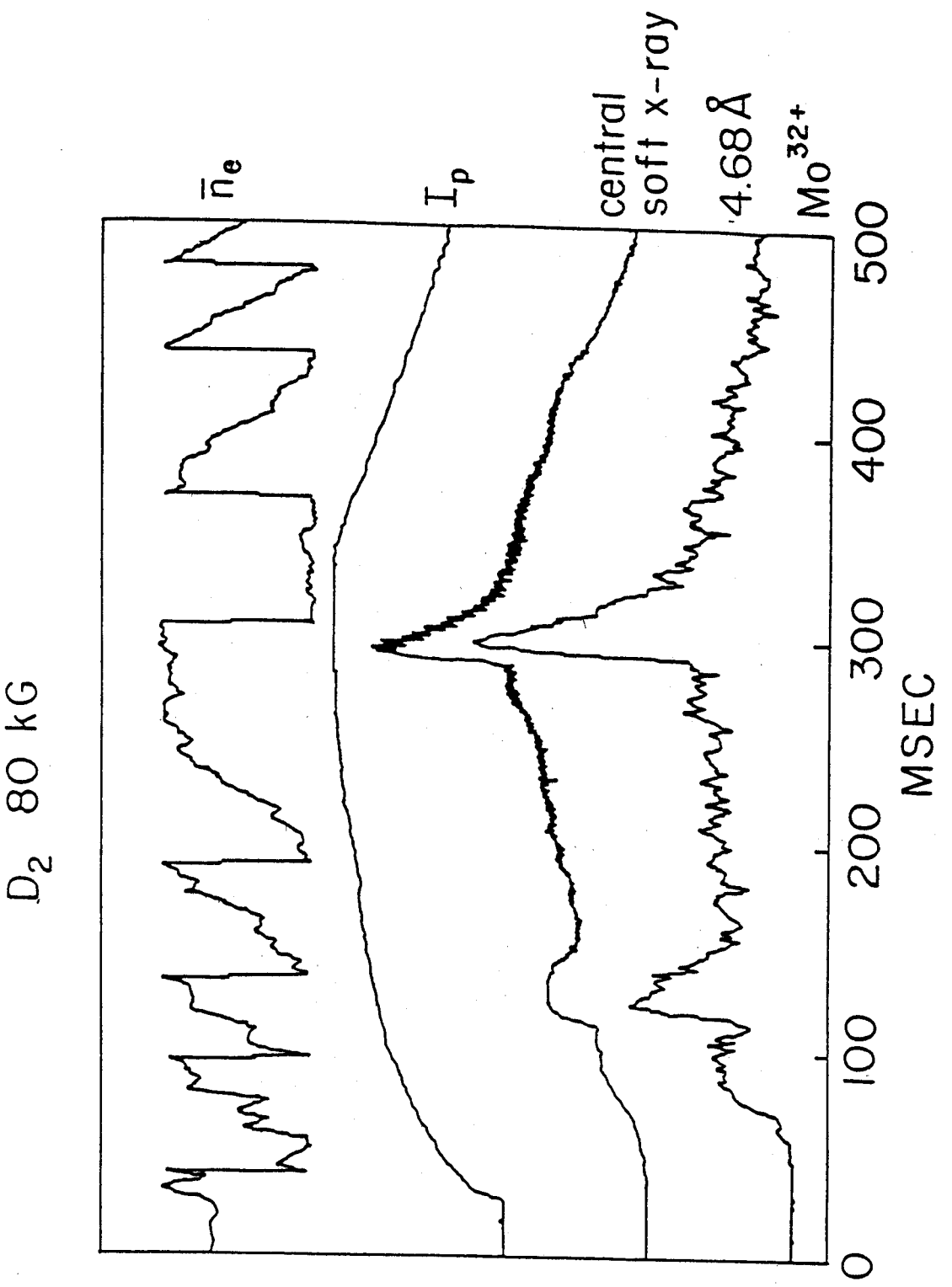
D_2 80 kG
$\bar{n}_e$
I_p
central soft x-ray
4.68 Å
Mo^{32+}
0
100
200
300
400
500
MSEC

FIGURE 11

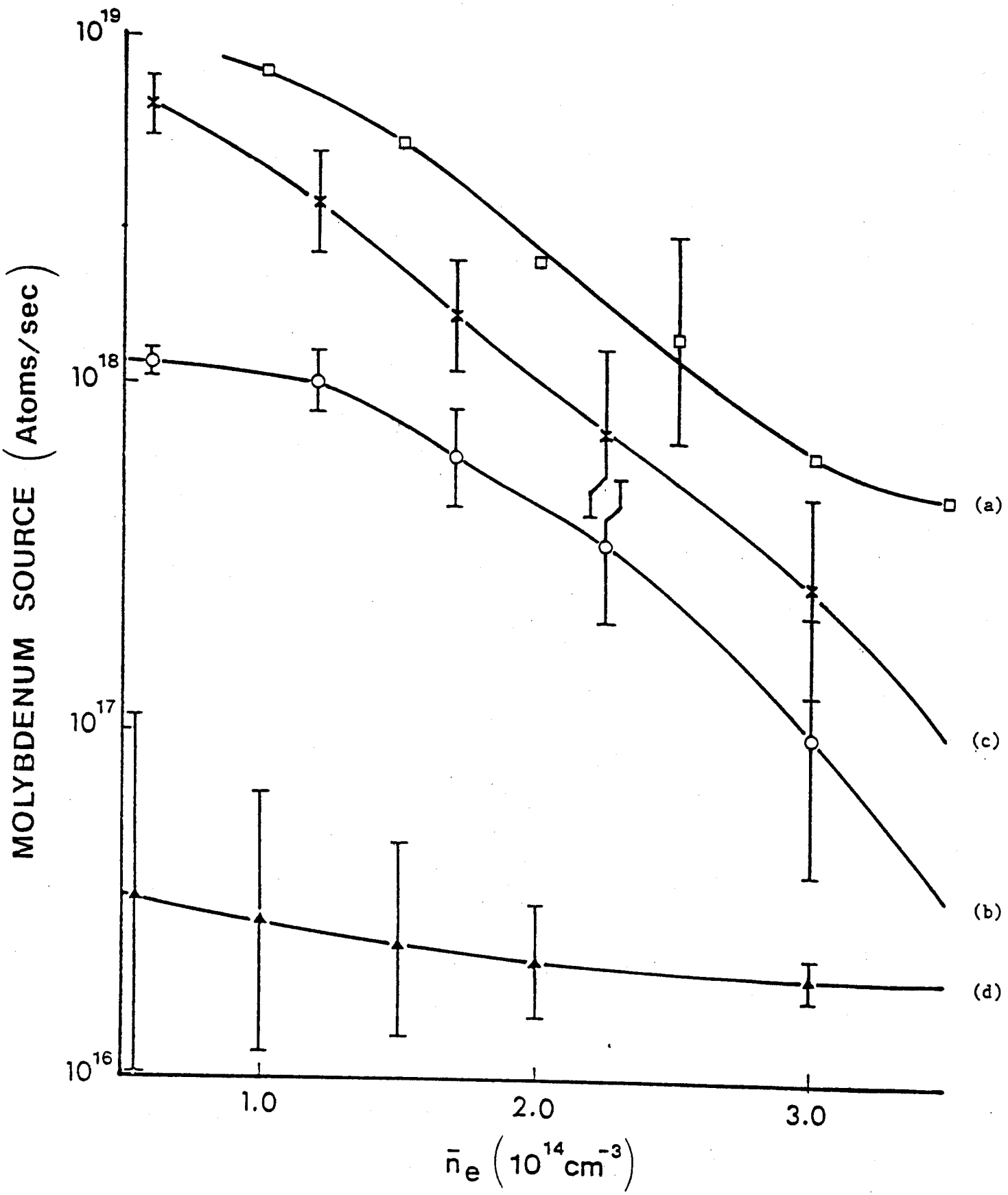
10^{19}
10^{18}
10^{17}
10^{16}
MOLYBDENUM SOURCE (Atoms/sec)
(a)
(c)
(b)
(d)
1.0
2.0
3.0
$\bar{n}_e$ (10^{14} cm^{-3})

FIGURE 12